Diffraction patterns have been simulated (Fig. 3 b, i to iii) for different degrees of ordering[5] of lithium and nickel ions between the layers (represented in Fig. 3 c, i to iii). Comparison with the initial diffraction pattern at 700 °C (Fig. 3 b, iv) shows that the lithium ions are essentially fully ordered between the layers. The unit cell is hexagonal, $R\bar{3}m$ with computed cell dimensions of $a = 2.904$ and $c = 14.36$ Å with a slight axial distortion away from the true cubic close packing ($c/a = 4.945$; ideal cubic = 4.899). This distortion is greater than at room temperature ($a = 2.885$, $c = 14.21$ Å, $c/a = 4.925$). The Figures 2 and 3 show that, during the initial period of catalytic activity the lithium nickel oxide structure remains invariant within the limits of our technique. The oxide appears to function as a uniform heterogeneous catalyst in the sense previously elaborated.[6]

In the second regime, 330–360 min, there is dramatic change; at least two crystallographic phases are present as the parent $Li_{0.46}Ni_{0.54}O$ is reduced to its daughter phase NiO (labelled b in Fig. 2). Accompanying the appearance of NiO there is a sharp rise in the degree of conversion of CH_4, and the principal product is CO_2. Production of C_2 hydrocarbons decreases to zero as the Li-Ni-O phase disappears.

In the third and final regime, 360 min and longer, metallic nickel (c in Fig. 2) along with some Li_2CO_3, is the predominant crystallographic phase. It is also noted that new, sharp peaks appear (labelled d); these are as yet unidentified and rapidly disappear (see top diffraction pattern of Fig. 2) before the catalyst is finally converted to metallic nickel and lithium carbonate. In this regime CO is the dominant gaseous product of catalytic reaction, and there is now no longer a uniform heterogeneous catalyst.

In summary, it has been shown that in situ X-ray diffractometry coupled with parallel gas chromatography throws fresh light on the structure of reactive solid catalysts. In the case of the Li-Ni-O system studied here, three distinct regimes could be readily identified each with different gaseous products. Furthermore, although the experimental conditions were not optimized, it was possible to detect the presence of an as yet unidentified transitory solid product as well as those expected on the basis of the known chemistry of the parent, monophasic mixed oxide catalyst. Greater time resolution may be attained with our set-up by using a higher flux of X-rays and a more sensitive detector.

Received: January 30, 1989

[1] M. Hatano, K. Otsuka, *Inorg. Chim. Acta 146* (1988) 243–247.
[2] R. K. Ungar, X. Zhang, R. M. Lambert, *Appl. Catal. 42* (1988) L1–L4.
[3] P. J. Maddox, J. Stachurski, J. M. Thomas, *Catal. Lett. 1* (1988) 191.
[4] L. D. Dyer, B. S. Borie, Jr., G. P. Smith, *J. Am. Chem. Soc. 76* (1954) 1499.
[5] J. B. Goodenough, D. G. Wickham, W. J. Croft, *J. Phys. Chem. Solids 5* (1958) 107.
[6] J. M. Thomas, *Angew. Chem. Int. Ed. Engl. 27* (1988) 1673; *Angew. Chem. 100* (1988) 1735.

The following short communications will be published in future issues: *D. Schweitzer et al:* Superconductivity at 7.5 K and Ambient Pressure in Polycrystalline Pressed Samples of β_p-(BEDT-TTF)$_2I_3$ – *R. Kniep et al:* Structure of Anodic Oxide Coatings on Aluminum – *G. Gray et al:* Siloxane Copolymers with Laterally and Terminally Attached Mesogenic Side Chains

High Resolution Electron Microscopy of the High-T_c Superconductor $Bi_{2+x}Sr_2Ca_{1-x}Cu_2O_{8+\delta}$

By *W. Zhou, A. I. Kirkland, K. D. Mackay, A. R. Armstrong, M. R. Harrison, D. A. Jefferson, W. Y. Liang* and *P. P. Edwards**

The structure of the 85 K Bi-Sr-Ca-Cu-O superconductor has been investigated by means of high resolution electron microscopy combined with image simulation. An ordered one-in-five substitution of calcium by bismuth ions is proposed as the explanation for the observed superlattice formation. This model is consistent with the reports of the recent analytical studies carried out on the same system.

The discovery of high temperature superconductivity in the Bi-Sr-Ca-Cu-O system has demonstrated conclusively that this phenomenon is not confined to compounds containing yttrium and rare-earth elements.[1–4] Several groups have isolated a high-T_c phase in this system and single crystal X-ray[4–6] and neutron diffraction[7] studies have shown both similarities and differences between these new cuprate superconductors and the previously known 40 K and 90 K materials.[4–6] A superstructure has also been observed in these diffraction studies and various structural models for its formation have been proposed.[8–10] Equally important was the indication of additional electron density at the Ca site suggesting a variable Bi:Sr:Ca occupancy.[5,6] Here the results of high resolution electron microscopy (HREM) and model image simulation of the title compound are presented from which an ordered compositional variation in atomic arrangement, which leads naturally to the superlattice for-

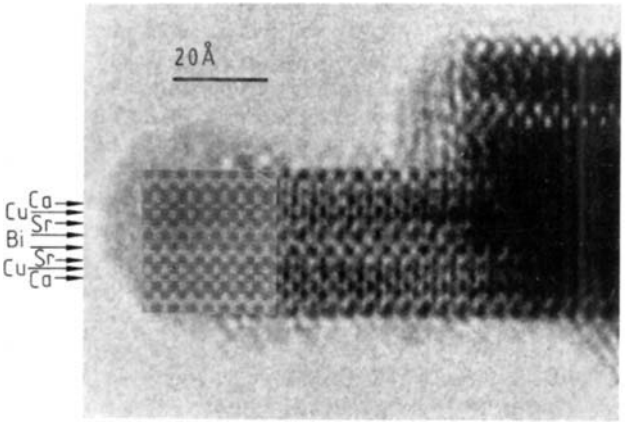

Fig. 1. HREM image of the tip of one crystal a single c lattice vector wide viewed down [110] of the published unit cell together with a calculated image inset (defocus = 950 Å, crystal thickness = 20 Å). The image clearly shows in cross section the metal layers in the order (Bi-Sr-Cu-Ca-Cu-Sr-Bi).

[*] Dr. P. P. Edwards, Dr. W. Zhou, Dr. A. I. Kirkland, Dr. K. D. Mackay, Dr. A. R. Armstrong, Dr. D. A. Jefferson, Dr. W. Y. Liang
Interdisciplinary Research Centre in Superconductivity
University of Cambridge
Madingley Road, Cambridge CB3 0HE (UK)
Dr. M. R. Harrison
General Electric Company
Hirst Research Centre
East Lane, Wembley, Middlesex HA9 7PP (UK)

[**] We thank the SERC, P.A. Technology (*W. Z.*), Alcan Chemical Ltd. (*A. I. K.*), and B.P. Research (*A. R. A.*) for financial support.

mation, is proposed. The substitution of Bi on the Ca site also leads to oxygen incorporation and concomitant oxidation.

The crystallites invariably possessed a plate-like morphology and images were readily obtained down the [001] zone axis. These images and electron diffraction patterns confirmed the essentially square 5.4 Å basic unit cell in this projection, and also indicated the pronounced superlattice. Some crystallites were also found to fracture perpendicular to their main cleavage plane or alternatively to curl up at the edges. It was then possible to obtain images in [110] or [100] projections. Figure 1 shows an image of a crystal in its [110] projection and the crystal is only one *c* lattice vector or unit cell wide. No evidence of the superlattice is visible in this projection. It appears that the projected charge density approximation[11] can be used to interpret the image and that the dark dots in the image can thus be correlated with the cation positions, although the oxygen atoms cannot be observed directly. The one-dimensional superlattice can be seen when the crystals are viewed in the [100] orientation, as shown in Figure 2. In this case the image is from the edge of a curled-

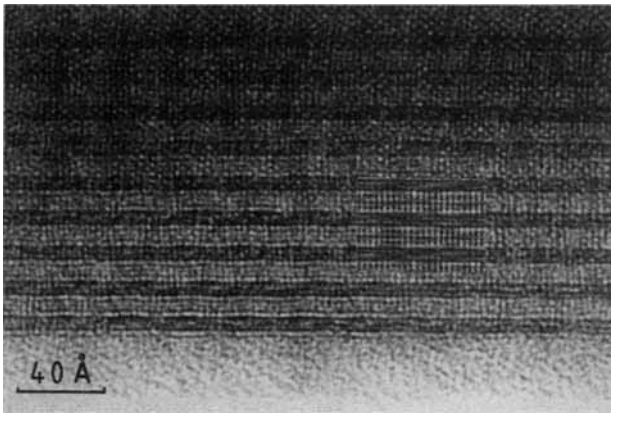

Fig. 2. HREM image of a crystal viewed down the [100] direction, with the one-dimensional superlattice being visible. The model simulation (insert) was calculated for a crystal thickness of 30 Å and an objective lens defocus of −1600 Å.

up platelet crystal some 200–300 Å thick, and clearly shows both the layer-like nature of the material, and a subtle variation of fringe contrast in a direction along the plane of the layers indicating the existence of the superlattice. No drastic variations in the basic arrangement of lattice fringes were observed, implying that a relatively minor effect, such as cation substitution or displacement may be responsible for the superlattice. In general, the superlattice was observed in one dimension as shown in Figure 3 a, but a two-dimensional variant was also observed in certain cases (Fig. 3 b). The periodicity of the superlattice, whether one- or two-dimensional is predominantly five basic cell repeats, though periods of four and six unit cells were also recorded. In addition, these superlattice vectors have occasionally been observed to be slightly inclined to the basic cell axes. No platelets were obtained which did not exhibit the superlattice.

Two structural models have been proposed[4–6] for this new high temperature superconductor based on single crystal X-ray studies. These models have virtually identical cation distributions, but differ in the arrangement of oxygen ions in the Bi_2O_2 bilayer. In the first,[4] oxygen ions are placed between the sheets of bismuth ions, in an arrangement similar to that found in Aurivillius layered oxides,[12] whereas the second[5–7] has a coplanar arrangement of bismuth and oxygen. The [110] projection is most suitable for comparing the two models, and accordingly images from both were simulated and compared with experimental results. At a focus slightly beyond the optimum both simulations gave a broad overall agreement with the features of the experimental image, although with the oxygens in the same plane as the bismuth the scattered intensity from this plane appeared to be slightly enhanced, and this manifested itself as a more pronounced white fringe between the bismuth-oxygen components and the rest of the structure. The differences between the simulations from the two models were, however, minimal and it was concluded that the scattering from the oxygen ions was insufficient at this value of specimen thickness to distinguish between them. However, with the onset of increased multiple scattering at greater specimen thicknesses differences were expected to occur,[13] but interpretation of images of thick crystals of such strong scatterers is difficult, particularly for those involving inelastic electrons.[14] In addition, there exists the possibility of crystal bending. Consequently no further attempts at image matching were made, although studies of this problem are continuing.

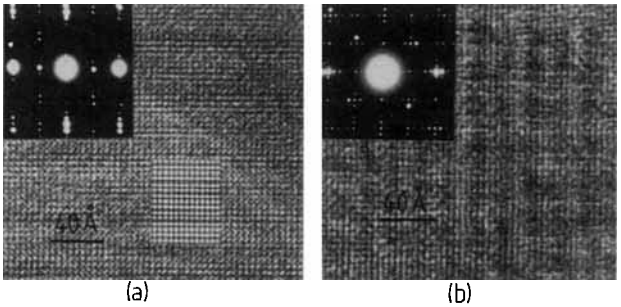

Fig. 3. HREM image of a crystal viewed in the [001] orientation, with insert selected area electron diffraction patterns, a) with one-dimensional superlattice, b) with an apparent two-dimensional superlattice. The inset image simulation in a) was calculated for a crystal thickness of 60 Å and an objective lens defocus of −2200 Å.

This same model was used to simulate images in the [100] projection and again it gave good agreement with the basic image contrast. However, in this projection a superlattice was also visible, which can be seen as a periodic darkening of the overall contrast in a direction perpendicular to the *b* axis (Fig. 2). Image simulations from the basic structure reveal that the darker component represents the Bi_2O_2 layer and the lighter parts the Sr-Ca-Cu-O. This darkening might therefore arise from the inclusion of heavier cations within the Sr-Ca-Cu-O component. Bearing in mind the established tendency of bismuth to replace calcium, it is proposed that this is the origin of the modulating image contrast. Accordingly a model was constructed for such a superlattice and this is shown schematically in Figure 4. Here rows of calcium ions parallel to the [100] axis were replaced by bismuth in

every fifth unit cell. The proposed substitution of the Ca by Bi ions will necessitate a conversion of the square pyramids of oxygen around copper atoms into linked octahedra which effectively constitute a small section of perovskite structure and will also require a local expansion of the structure in the [001] direction. Between the regions of additional bismuth, the layers in the model of Figure 4 suffer a contraction, and, as the regions of excess bismuth are staggered in adjacent layers, the average layer spacing is that of the published structure. Interestingly in this construction, each Bi substituent is accompanied by two oxygen atoms which over-compensate for the increased charge on the bismuth. Thus the resultant stoichiometry is $Bi_{2.2}Ca_{0.8}Sr_2Cu_2O_{8.4}$, giving a nominal average copper valency of +2.33, reminiscent of the copper valency in $YBa_2Cu_3O_7$ superconductors. Images simulated from this model are in good agreement with those obtained experimentally in the [001] projection (Fig. 3). The same model was also used to simulate images in the [100] projection with some displacement/relaxation of the anion lattice at the positions of the inserted oxygen ions as indicated in Figure 4, and the basic superlattice contrast was again obtained. It is therefore concluded that this substitution scheme provides a plausible explanation for both the non-stoichiometry of this material and the observed superlattice. Furthermore, it is assumed that the occasional departure of the superlattice period from five to either four or six unit cell repeats is a means by which the lattice can reduce the strain energy built up by this distortion.

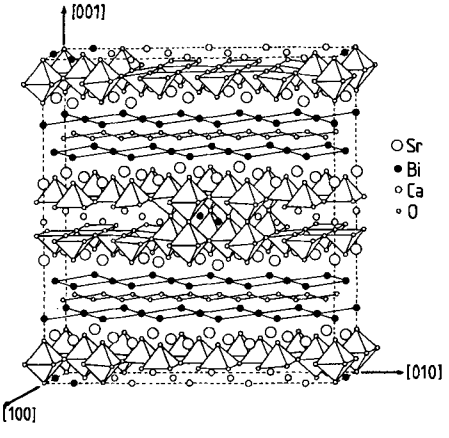

Fig. 4. One superlattice unit cell of the structure model used for the image simulations of Figures 1, 2 and 3. The copper atoms are located at the centers of the square pyramids or octahedra. Unit cell dimensions are $a = 5.4$ Å, $b = 5.4$ Å, $c = 30.7$ Å.

In compositional terms, our model is consistant with the analytical data of *Chippindale* et al.,[15] and would correspond to their predominant phase. Detail differences in cation ratio could well arise from the presence of the superlattice and its variable periodicity, and our structure model can be regarded as an intermediate between two possibly hypothetical end-member phases, namely $Bi_2CaSr_2Cu_2O_8$ and $Bi_3Sr_2Cu_2O_9$. With the general formula $Bi_{2+x}Ca_{1-x}Sr_2Cu_2O_{8+2x}$, the main phase described by *Chippindale* et al.[15] would correspond to $x = 0.143$. On the other hand, their second phase cannot fit easily into this scheme due to the much reduced copper content. This phase, which has a reduced c parameter, may be constructed, however, if a complete Cu-O layer together with a Sr-O layer, were removed, giving the stoichiometry $Bi_{2+x}Ca_{1-x}SrCuO_6$, with $x = 0.286$.

Experimental

Samples with nominal stoichiometry $Bi_{2+x}Sr_2Ca_{1-x}Cu_2O_{8+\delta}$, where $x \approx 0.2$ and $\delta \approx 0.4$, were prepared by reacting Bi_2O_3, $CaCO_3$, $SrO_2/Sr(NO_3)_2$ and CuO in appropriate proportions at 800 °C in air for 20 hours. Samples were tested for superconductivity in the temperature range 10–300 K using both four-probe electrical resistance and field exclusion measurements, and the results in Figure 5 show that a zero resistance state is obtained at 83 K. The samples showed a Meissner effect comparable to those obtained for $YBa_2Cu_3O_{6.9}$ in the same apparatus.

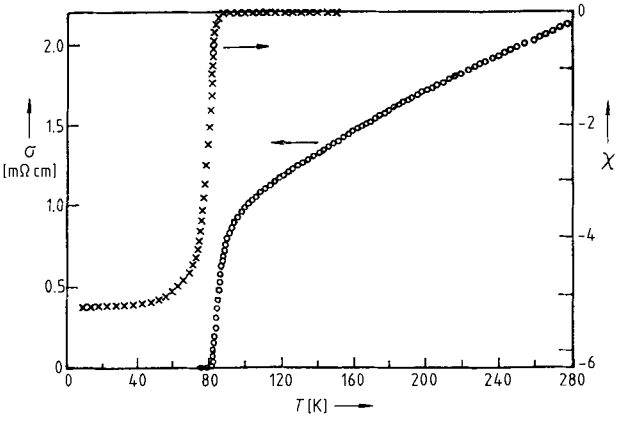

Fig. 5. Variation with temperature of resistivity and AC susceptibility of a pressed pellet of $Bi_{2+x}Ca_{1-x}Sr_2O_{8+\delta}$, where nominally $x \approx 0.2$ and $\delta = 0.4$. The resistivity vanishes at 83 K coinciding with the sharp turn in the susceptibility.

Specimens were prepared for HREM examination by grinding the synthesized material in an agate mortar and pestle in either acetone or liquid nitrogen; the latter being used to embrittle the sample and encourage non-standard cleavage. A drop of the suspension was then placed onto a copper grid coated with a holey carbon film. HREM investigations were carried out with a modified JEOL JEM-200CX instrument [16] operated at 200 kV, with objective lens characteristics $C_s = 0.52$ mm, $C_c = 1.05$ mm and an interpretable point resolution of 1.95 Å at the optimum defocus. Crystals were chosen by examination in the selected-area diffraction mode, and they were oriented such that the beam was parallel to each of the main high symmetry zone axes. After careful correction of residual astigmatism and illumination system misalignments [17], images were recorded at a magnification of ca. 450.000 X. For comparison with experimental images, model-simulated images were computed using the multislice method [18] for [100], [110] and [001] projections of the previously identified basic unit cell over a systematic range of crystal thicknesses and objective lens defocus values.

Received: November 8, 1988;
supplemented version: March 20, 1989

[1] C. Michel, M. Hervieu, M. M. Borel, A. Grandin, F. Deslandes, B. Raveau, *Z. Phys. B68* (1987) 421.
[2] H. Maeda, Y. Tanaka, M. Fukutomi, T. Asano, *Jpn. J. Appl. Phys. Lett. 27* (1988) L 209.
[3] C. W. Chu, L. Gao, P. H. Hor, Z. J. Huang, R. L. Meny, Y. Y. Sun, Y. Q. Wang, Y. Y. Xue, *Phys. Rev. Lett. 60* (1988) 941.
[4] M. A. Subramanian, C. C. Torardi, J. C. Calabrese, J. Gopalkrishnan, K. J. Morrisey, T. R. Askew, R. B. Flippeu, U. Chowdhry, A. W. Sleight, *Science 239* (1988) 1015.

[5] S. A. Sunshine, T. Siegrist, L. F. Schneemeyer, D. W. Murphy, R. J. Cava, B. Batlogg, R. B. van Dover, R. M. Fleming, S. H. Glarum, S. Nakahara, R. Farrow, J. J. Krajewski, S. M. Zahurak, J. V. Waszczak, J. H. Marshall, P. Marsh, L. W. Rupp, Jr., W. F. Peck, *Phys. Rev. B38* (1988) 893.
[6] J. M. Tarascon, Y. Le Page, P. Barboux, B. G. Bagley, L. H. Greene, W. R. McKinnon, G. W. Hull, M. Giroud, D. M. Whang, *Phys. Rev. B37* (1988) 9382.
[7] H. G. von Schnering, L. Walz, M. Schwarz, W. Becker, M. Hartweg, T. Popp, B. Mettich, P. Müller, G. Kämpf, *Angew. Chem. Int. Ed. Engl. 27* (1988) 574; *Angew. Chem. 100* (1988) 604.
[8] Y. Matsui, H. Maeda, Y. Tanaka, S. Horiuchi, K. Ibe, *Inst. Phys. Soc. Conf. Ser. 93* (1988) 231.
[9] L. R. Wallenberg, J. S. Anderson, J. G. Thompson, R. L. Withers, J. D. Fitzgerald, *Inst. Phys. Soc. Conf. Ser. 93* (1988) 237.
[10] M. D. Kirk, J. Nogami, A. A. Baski, D. B. Mitzi, A. Kapitulnik, T. H. Geballe, C. F. Quate, *Science 243* (1988) 1673.
[11] D. F. Lynch, M. A. O'Keefe, *Acta Crystallogr. A28* (1972) 536.
[12] B. Aurivilius, *Arh. Kemi. 2* (1950) 519.
[13] N. P. Huxford, D. J. Englesham, C. J. Humphreys, *Nature London 329* (1987) 812.
[14] W. O. Saxton, W. M. Stobbs, *J. Microsc. 151* (1988) 171.
[15] A. M. Chippindale, S. J. Hibble, J. A. Hriljac, L. Cowey, D. M. S. Baggley, P. Day, A. K. Cheetham, *Physica C152* (1988) 198.
[16] D. A. Jefferson, J. M. Thomas, G. R. Millward, K. Tsuno, A. Harriman, R. D. Brydson, *Nature London 323* (1986) 428.
[17] D. M. Smith, W. O. Saxton, M. A. O'Keefe, G. J. Wood, W. M. Stobbs, *Ultramicroscopy 11* (1983) 263.
[18] J. M. Cowley, A. F. Moodie, *Acta Crystallogr. 10* (1957) 609.

Polymer Benzo[15]crown-5 Complexes as Sensor Materials for Solvent Vapors—Aromatic Halogenated Hydrocarbons and Polar Solvents**

By *Franz L. Dickert** and *Doris Zeltner*

Dedicated to Professor Gerd Wedler on the occasion of his 60th birthday

For the first time thin layers of polymer-metal complexes with crown ether ligands have been applied as sensor materials for the detection of solvent vapors. The hydrophobic properties of these films enable the detection of even halogenated and aromatic hydrocarbons through conductivity measurements.

The crown ether[1] [15]crown-5 (15C5) forms 1:1 complexes with Mg^{II}, Zn^{II}, Co^{II} and Ni^{II} ions (because they fit well into the cavity of this macrocyclic ligand) and can act as a tetra- or pentadentate ligand.[2, 3] Complexes with the composition $[M^{II}(15C5)(S)_2]^{2\oplus}$ have been identified in donor solvents (S). In inert solvents, however, even the usually non-coordinating $ClO_4^{\ominus}$ ion yields inner sphere complexes.[3] The reversible substitution reaction of coordinated anions $X^{\ominus}$ (e.g. $ClO_4^{\ominus}$) by donor molecules [Eq. (a)] has been applied to develop sensor materials for solvent vapors:

$$[M^{II}(15C5)(X)_2] + 2\,S \rightleftharpoons [M^{II}(15C5)(S)_2]^{2\oplus} + 2\,X^{\ominus} \qquad (a)$$

[*] Prof. Dr. F. L. Dickert, Dr. D. Zeltner
Institut für Physikalische und Theoretische Chemie
der Universität Erlangen-Nürnberg
Egerlandstraße 3, D-8520 Erlangen (FRG)

[**] This work was supported by Siemens AG, Central Research and Development (ZFE F1 AMF 32, Dr. G. Mages), and the Fonds der Chemischen Industrie.

The formation of a charged complex and anions through the interaction of the initial complex with solvent molecules can easily be detected by conductivity measurements. For practical use formaldehyde resins[4] synthesized from benzo[15]crown-5 (B15C5) are more convenient (§B15C5). These polymer materials form complexes with $Mg^{2\oplus}$ such as **1** in $CH_3OH/CHCl_3$ solution.

Solutions of these polymer complexes are dropped onto interdigital structures to perform conductivity measurements. Stable amorphous films with a thickness of approximately 0.2 μm to 1 μm are obtained after evaporation of the solvent.

The sensor effect consists of two steps. First, an absorption of solvent vapors by the solid macrocyclic layers occurs followed by a chemical reaction according to equation (a). Macrocyclic complexes are very favorable materials for the absorption of different kinds of solvent since these ions have pronounced hydrophobic properties. Strong absorption occurs in the case of protic and aprotic polar solvents such as alcohols, ketones, esters etc. and also for aromatic and halogenated hydrocarbons.

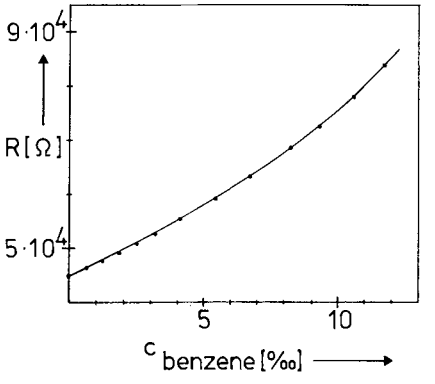

Fig. 1. Dependence of the resistance of the 1:1 complexes of $Mg(ClO_4)_2$ with §B15C5 on an interdigital structure (5 μm electrode distances) on the amount of benzene in the air at 20 °C and 50% humidity.

A typical measurement, e.g. the detection of benzene in the air, is depicted in Figure 1. The resistance of the sensor layers increases parallel with the amount of solvent vapor in the air produced by a gas mixing apparatus.[5] Solvents with no donor properties also result in this sensor effect, since water stemming from the humidity of the air is removed from the sensor layers by the incorporated benzene. Since ionic conductivity is responsible for the described effect, as the ion concentration is diminished according to equation (a) the resistance of the sensor layers increases. The sensitivity of the proposed sensor materials to water vapors can be reduced by increasing the hydrophobic properties of the layers. This can be achieved by the inclusion of cross linking agents such as anisole which enlarge the aromatic ring content in the resins. The addition of ingredients with solvating power such as polyethyleneglycols enables sensors to be designed with characteristic properties. As shown in Figure 2 this procedure can yield a zero slope for certain solvent vapors (e.g. dichloromethane) whereas other solvents (e.g. ethanol) give